DESIGN CONSIDERATIONS AND INITIAL PERFORMANCE OF A 1.2cm^2 BETA IMAGING INTRA-OPERATIVE PROBE

Martin P. Tornai, Lawrence R. MacDonald*, Craig S. Levin, Stefan Siegel, Edward J. Hoffman

Division of Nuclear Medicine & Biophysics, Department of Molecular and Medical Pharmacology, UCLA School of Medicine, Los Angeles, CA 90095

**Department of Physics, UCLA, Los Angeles, CA 90024*

ABSTRACT

A novel small area beta ($\beta^{\pm}$) detector is under development for nuclear emission imaging of surgically exposed radiolabeled tumor beds. The imaging device consists of an 0.5 mm thick x 1.25 cm diameter $CaF_2(Eu)$ scintillator disk coupled to a rigid bundle of 19, 2 mm diameter x 5 cm long double clad optical fibers through a 1.7 mm polystyrene light diffuser. The detector size (1.2 cm^2) was determined by the requirement to introduce the probe into small cavities, e.g. during neuro-surgical lesion resection, but large enough to produce images of clinical significance. Double clad optical fibers were utilized for both the front- and back-end components, and ~75 photoelectrons were obtained through a 1.9 m long flexible optical fiber bundle with $CaF_2(Eu)$, indicating that sufficient numbers of photoelectrons were detected at the PMT for positioning and energy information. The long flexible fibers guide the scintillation light to a Philips XP1700 series fiber optic faceplate, multi-channel PMT. The parallel MC-PMT outputs are fed into a variable gain, charge divider network and an *i*-V pre-amplifier/line driver network, whose resulting four outputs are digitized and histogrammed with standard Anger positioning logic. The various components in the imaging chain were optimized by both simulations and measurements. Line spread functions measured in the 10.8 mm FOV were 0.50 mm ± 0.038 mm and 0.55 mm ± 0.065 mm FWHM, in X and Y, respectively. For a 20% variation in pulse height, no variation in spatial resolution was observed. The differential uniformity was measured to be ±15.6% with ~150 cts/pixel.

I. INTRODUCTION

A novel small area (1.2 cm^2) beta ($\beta^{\pm}$) detector, which overcomes many of the problems associated with gamma-ray detection and imaging [1,2], is under development (Fig. 1) for nuclear emission imaging of intra-operatively exposed, radiolabeled tumor beds [3-7]. The beta imaging probe is intended to delineate the boundaries of radiolabeled tumors, after the bulk of the lesion has been removed. Direct intra-operative detection of short ranged $\beta^{\pm}$ particles is not a new technique [8,9]. However, intra-operative imaging greatly facilitates the mapping of radioactive distributions on tissue surfaces and would aid a surgeon in residual lesion identification for removal, while sparing unaffected tissues. The technique exploits: (1) the inherent short range of $\beta^{\pm}$ particles in tissue; (2) direct source contact obviating a collimator; and (3) detector to source proximity, which has the dual advantage of increased sensitivity [2] and improved resolution [10,11] in nuclear emission imaging. The success of the beta imaging device depends on detecting a sufficient number of scintillation photons through ~2 m of flexible optical fibers at a remotely located photodetector. The optical fibers facilitate miniaturization of the imaging system, and remove all voltage and current sources from the surgical field.

II. DETECTOR COMPONENTS

A. Light Sharing Scintillation Detector

A continuous disk of $CaF_2(Eu)$ scintillator was optimized for <1 MeV $\beta^{\pm}$ particles [6], since use of the device is anticipated with ^{18}F (β^+ $E_{\beta\,max}$ = 635 keV) labeled pharmaceuticals.

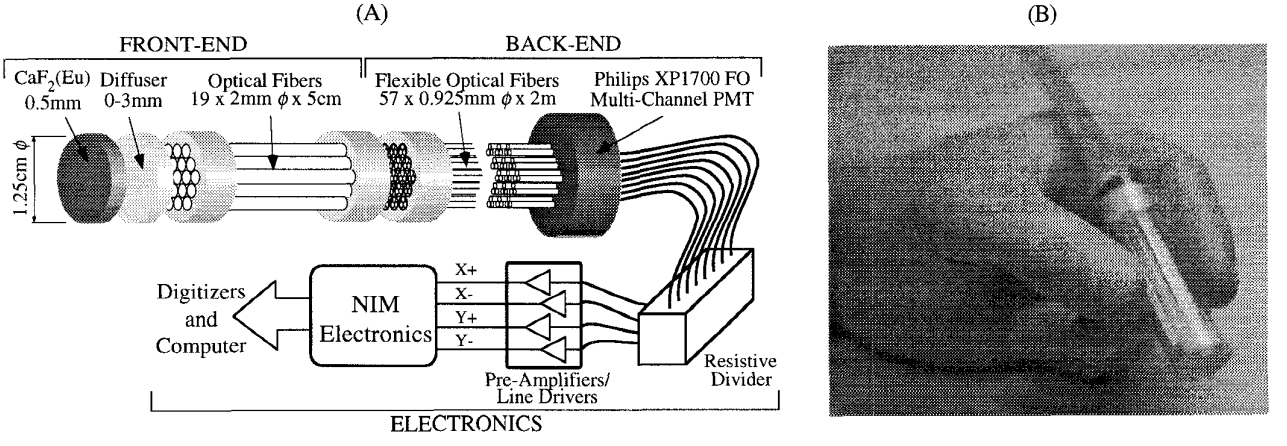

FIGURE 1. (A) Schematic diagram of the beta imaging intra-operative probe. The front-end components are intended to be glued together, and as a unit are removable, sterilizable and exchangeable for other application dependent front-end geometries. Discrete scintillators can be substituted for the continuous disk scintillator as desired. The flexible back-end components and electronics are designed to be universally adaptable to various front-end components. (B) Scale photograph of the actual device described in this paper.

0-7803-3180-X/96$5.00©1996

$CaF_2(Eu)$ has a low refraction index (n=1.44) which assists in efficient light transfer into optical fibers. The slow decay time (940 μsec) is not anticipated to be a problem as low *in vivo* count rates (~100 cps) are expected. A 0.5 mm thick x 1.25 cm diameter (ϕ) geometry $CaF_2(Eu)$ crystal was found to have the best properties in terms of light output, and minimal contribution from background (e.g. from 511 keV annihilation gammas if β^+ are detected) [6]. Various energy calibration techniques were investigated for the thin scintillators intended for use in the device [4,5,7].

B. Diffusing Light Guide

The light diffuser (Fig. 1A) is an important component that controls scintillation light spread among the front-end fiber optic elements. The type and geometry of light diffuser affects both the light transmission from the scintillator into the front-end fibers, and also the spatial resolution of the device. Too great a spread in the light allows for a high background in the tails of the light spread and decreases positioning accuracy [12,13]; too small a spread discretizes a continuously positioning detector into the number of front-end elements [4].

Pulse height measurements were made with the thin $CaF_2(Eu)$ scintillator coupled to various thicknesses of clear polymethylmethacrylate (PMMA, n=1.49) and polystyrene (PS, n=1.58) light guides (0.5-3.0 mm) coupled through a front-end bundle of 19, 2 mm ϕ double clad PS (DCPS) fibers in a white PMMA holder (Fig. 1), and irradiated with ^{204}Tl (β^- $E_{\beta\,max}$ = 763 keV) (Fig. 2). The ~10% pulse height difference between PS and PMMA light guides indicates that the better refraction index match for PS between the scintillator and front-end fibers plays a greater role than the small transmission variation of the materials ($T_{PS} < T_{PMMA}$ by about 6%).

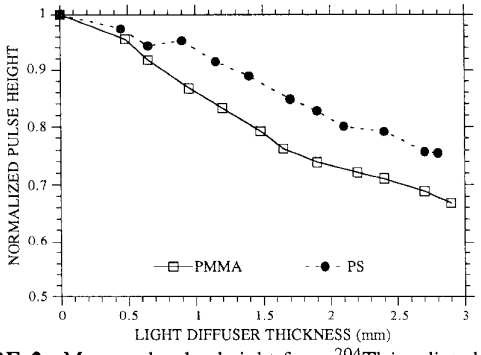

FIGURE 2. Measured pulse height from ^{204}Tl irradiated 0.5 mm thick $CaF_2(Eu)$ disk, covered with Teflon, through PMMA and PS light guides coupled via bundle of 19, 2 mm ϕ x 10 cm DCPS fibers to multi-channel PMT.

C. Front-End Fiber Optics

The best front-end optical fiber was determined from the measured transmission properties of eight 2 mm ϕ fibers with various numerical apertures (NA=0.4-0.72) and core materials (PS, PMMA, glass, quartz).

Fibers (30 cm long) were attached with optical grease to the $CaF_2(Eu)$ scintillator (covered with a layer of Teflon) through a white PMMA fiber holder and also through a hole on a black faceplate to an RCA C31024 PMT. The PMT gain was calibrated with single photoelectron (PE) measurements [14]. The measured pulse height with ^{204}Tl beta irradiation (Fig. 3) was calculated as the weighted mean of the beta distribution, which was shown to be a reliable indicator of the mean light output from thin scintillators [7]. As the NA increased, the total number of detected PEs also increased, which is consistent with the greater acceptance angle (NA) of the fiber.

The DCPS plastic optical fiber (Kuraray Int'l) was determined to have the best properties, both in terms of light transmission for $CaF_2(Eu)$ light, and material composition. The DCPS fiber is a multi-mode, step index double clad PS core fiber (n_{core}= 1.59, $n_{inner\ clad}$= 1.49, $n_{outer\ clad}$= 1.42). The outer fluorinated polymer cladding in the DCPS optical fibers ensures an excellent first cladding surface, relatively free of imperfections [3,15].

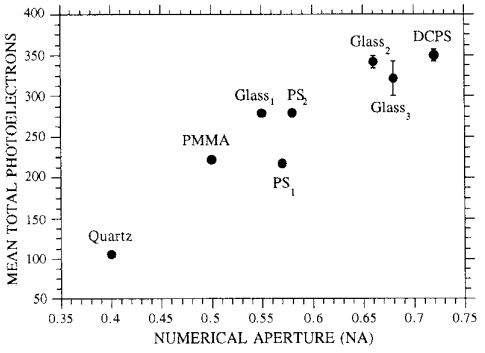

FIGURE 3. Measured mean total PEs for $CaF_2(Eu)$ light through various core material, 2 mm ϕ optical fibers. PMMA=polymethylmethacrylate, PS=polystyrene, DCPS=double clad PS. Subscripts indicate different material compositions.

D. Detector & Fiber Structural Support

The 19 input fibers are held in a close packed hexagonal arrangement maximizing surface coverage (Fig. 1). This is a standard, close packed PMT arrangement for Nuclear Medicine gamma cameras [10,11,16]. Three holders, 5 mm thick x 1.25 cm ϕ with 2 mm ϕ holes, were tested: PMMA (white, black), and aluminum. 5 cm long DCPS optical fibers were glued into each holder and polished. These holders are removable from the back-end fiber optics (Fig. 1) and are intended to be exchangeable with various geometry front-ends developed for specialized surface imaging applications.

The pulse height with different fiber bundle holders in the optimal imaging device (see section *E.*) was characterized with a 1.7 mm thick PS diffusing light guide between the scintillator and fiber bundle. Normalized to the white holder response, the pulse height variation was 1.0 ± 0.6%, 0.91 ± 0.3%, and 0.74 ± 0.2% for the white, black and Al holders, respectively.

E. Back-End Fiber Bundles

The optimum back-end fibers were also chosen to be DCPS fiber due to the overall excellent transmission properties with $CaF_2(Eu)$ ([3,15] and Fig. 3). The expected length is ~2m. Back-end fiber holders are identical to the front holders.

Three diameters of DCPS optical fibers were tested: 0.835 mm, 0.925 mm, and the reference 2.0 mm ϕ fibers. Tests were conducted by bundling and optically cementing four 0.835 mm, or three 0.925 mm, or single 2.0 mm ϕ fibers, all 15 cm long, into a white PMMA holder (Fig. 4). The total

light output was measured with the 0.5 mm thick $CaF_2(Eu)$ disk covered with Teflon and optically coupled to a 2 mm ϕ x 5 cm DCPS fiber and white holder flanged to the respective back-end test "bundles" (Table 1). The differences seen between the short (15 cm) fiber bundles is less than that expected for longer lengths (190 cm) because of increased multiple reflections in the smaller ϕ fibers.

When the light output was measured with the 1.9 m lengths, larger differences resulted (Table 1). Even though there was a 60% transmission loss in going from the long, inflexible yet optimal 2 mm ϕ back-end fiber to the more flexible, three 0.925 mm ϕ back-end fibers, a large number of PEs was detected at the PMT. Order of 70 PEs has been shown to be sufficient for use in energy and positioning information [3,4,11,16].

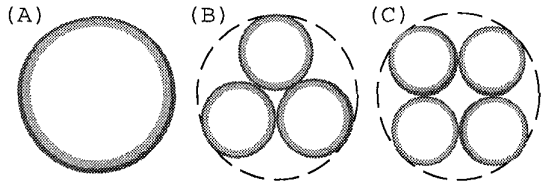

FIGURE 4. Various fiber arrangements for the back-end fibers inscribed in 2 mm ϕ holder. (A) 2.0 mm ϕ reference fiber; (B) 3 x 0.925 mm ϕ fibers and (C) 4 x 0.835 mm ϕ fibers.

TABLE 1. Comparison of light transmissions for $CaF_2(Eu)$ scintillator through various length "bundles" of back-end fiber optics. Errors shown are for multiple measurements (15 cm) and PE statistics (190 cm).

# Fibers	Diameter (mm)	Area Ratio	Mean Total PEs (±σ) 15 cm	190 cm
1	2	1	288.1 ± 44.5	180.8 ± 13.4
3	0.925	0.642	208.1 ± 2.9	73.3 ± 8.6
4	0.835	0.697	205.3 ± 12.8	-

F. Multi-Channel Photomultiplier

To identify the optimum placement of the back-end fibers on the photon detector elements or pixels, the optical and inherent electronic crosstalk properties of two multi-channel (MC) PMTs were evaluated. The Philips XP1702 and XP1722 [17] are 64 channel (8 x 8 pixels, each 2.54 mm on a side) MC-PMTs with bialkali photocathodes, differing in their optical input windows: the XP1702 has a continuous boro-silicate glass faceplate ~3 mm thick (T = 95% from 320-800 nm), and the XP1722 has an ~5 mm thick fiber optic (FO) faceplate (T = 70% from 390-800 nm).

2D Point spread function measurements were performed on both MC-PMTs illuminated with a green LED (~500 nm) through a 50 cm long x 0.835 mm ϕ DCPS fiber (NA=0.72). The fiber was raster scanned with an XYZ-translation stage in 0.5 mm regular increments around the inner 16 pixels of the 8 x 8 discrete pixel arrays of both MC-PMTs. 1000 events were collected per LED/fiber position. It was estimated that >100 PEs were produced at the photocathode of either PMT. The spatial responses of the MC-PMTs had pixel FWHMs of 3.18 mm ± 0.038 mm and 2.20 mm ± 0.16 mm for the XP1702 (glass) and XP1722 (FO) respectively (Fig. 5). Note the sharper delineation of the pixel in the FO faceplate MC-PMT which implies lower crosstalk between adjacent horizontal, vertical and diagonal elements.

The total light collected at a pixel-of-interest, normalized by the transmission properties of the MC-PMT faceplates (at ~500 nm) was 28.7% and 31.0% (±5.6% for both MC-PMTs) for the XP1702 and XP1722, respectively. The surprising result was that the XP1722 MC-PMT had approximately the same total pixel signal as the XP1702. Minimal signal crosstalk is very important for processing the discretized (fiber) signals from the front-end light sharing detector, as used in this imaging device.

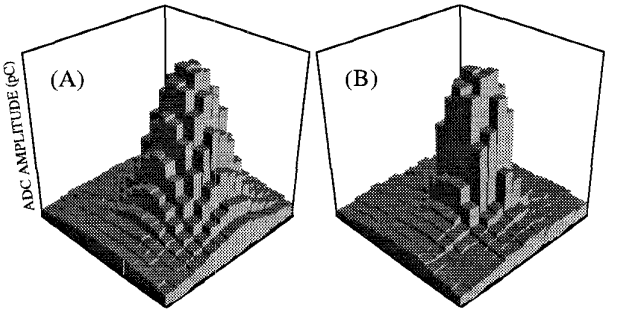

FIGURE 5. 2D PSF histogram of a 2.54 mm square pixel on the XP1702 (A) and XP1722 (B) MC-PMTs. Each amplitude (in the 16 x 16 histogram) represents the pixel's response with the input LED/fiber at a different location on the inner 16 pixels of the MC-PMT. All blocks are 0.5 mm apart in X and Y.

G. Positioning Readout Electronics

A simple charge division readout scheme [4,18] was developed and optimized for the imaging probe. The readout consists of a resistor network with four resistors, whose fixed values correspond to the Cartesian locations of the front-end optical fibers attached to a pixel element from the MC-PMT [11]. A fifth, variable resistor is also connected to each element and bleeds charge to ground, allowing gain balancing of each pixel in the imaging array. The positioning equations were the standard Anger logic equations, where each dimension (X or Y) is normalized by its own total signal (Fig. 6).

The four resistors from each pixel element are bused together depending on their X_+, X_-, Y_+, or Y_- location, and the resultant divided charge from each element is fed to a preamplifier, with 2 μsec shaping (feedback), and 50 Ω line driver.

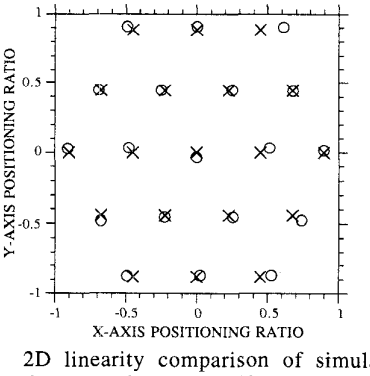

FIGURE 6. 2D linearity comparison of simulated optimal positions (X) and measured positions (O). The measured results were made with ±5% resistors.

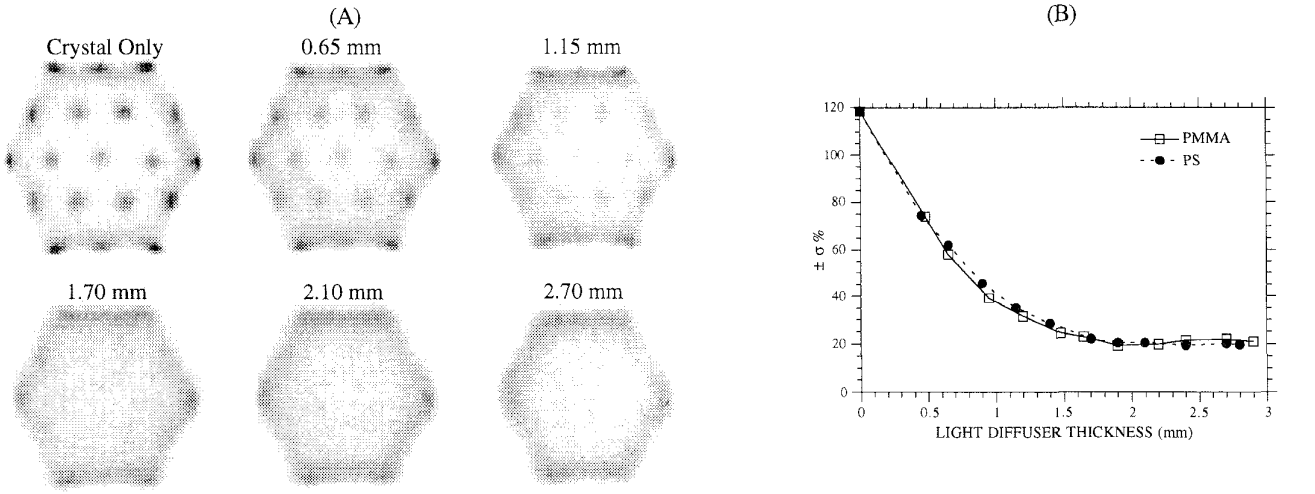

FIGURE 7. (A) Six images (64 x 64 pixels, 256 gray levels) of the flood field responses of the beta imaging device with $CaF_2(Eu)$ coupled to DCPS optical fibers with or without PS light diffusers. (B) Differential uniformity measured for PMMA and PS light diffusers as a function of thickness. $\pm\sigma$ % is measured as the standard deviation from the mean pixel value in the CFOV.

The resultant voltage signals were further amplified, shaped, discriminated and digitized with standard NIM and CAMAC electronics. Data acquisition control, analysis and image processing were performed on list mode data with a Macintosh IIfx platform using LabVIEW™ (National Instruments), and a VAX4000 system.

III. IMAGING CHARACTERISTICS

A. *Light Sharing & Uniformity*

The thickness and transmission of the light diffuser are critical to the spatial and uniformity response of the imaging device. As the thickness of the light diffuser increases (Fig. 7A), the pseudo-discretized imaging device becomes one that can image continuously between the 19 front-end fiber elements. The edge effects in this device are common to light sharing gamma camera systems [10]. The flood field responses of the PMMA and PS light diffusers were similar.

With a 1.7 mm thick PS light guide, the fiber "hot spots" just disappear in a gain balanced flood field image. Moreover, as the light diffuser thickness increases, the uniformity ($\pm\sigma$ % is the variation from the mean pixel value) in the center field of view (center FOV ≈ 75% area in the center of flood image) improves dramatically (Fig. 7B). Although the best uniformity was just <20% with ~36 cts/pixel in the image, which leads to 17% statistical error, when >150 cts/pixel were acquired, the uniformity improved to ±15.6% (with an 8% statistical error).

B. *System Spatial Resolution*

The system spatial resolution was measured with a ^{204}Tl source collimated through a 0.1 mm slit in a 1 cm thick black PMMA collimator directly in contact with the front surface of the imaging detector. The white fiber holder was utilized. This line source was stepped in the X and Y dimensions in 1.0 mm increments. Profiles were drawn perpendicular to the resultant line images and fit with Gaussians.

The surprising result obtained is, clearly, that the spatial resolution does not degrade with increased light sharing (Fig. 8A). Furthermore, for the PS thicknesses tested, there was an ~20% decrease in pulse height (Fig. 2) but no degradation in spatial resolution. For 2 m lengths of fiber, where we expect factors of 4 lower light (Table 1), this same 20% variation is expected to become a larger effect in spatial resolution.

With the 1.7 mm thick PS light diffuser, the spatial resolution was also measured for the various fiber holders (Fig. 8B). The spatial resolution improved from 0.58 mm ±

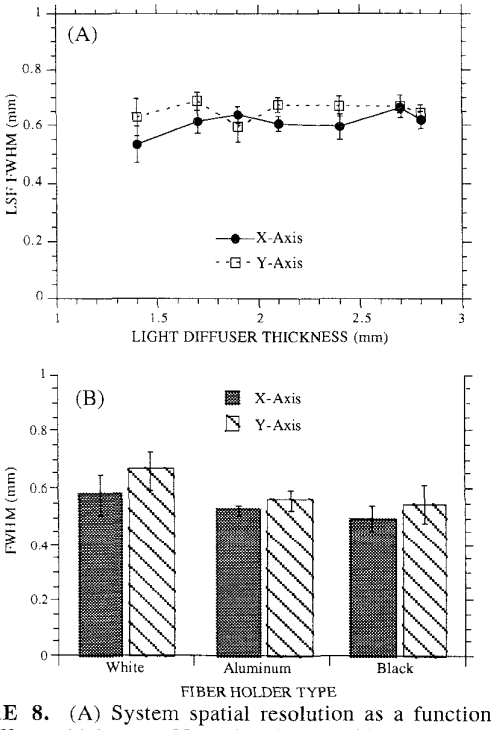

FIGURE 8. (A) System spatial resolution as a function of PS light diffuser thickness. Note that for the thicknesses indicated, there is an ~20% drop in pulse height with no significant effect on resolution. The white fiber holder was used with PS light diffusers. (B) Measured system spatial resolution for a 1.7 mm PS diffuser. There is an improvement in spatial resolution due to the absorptive properties of the fiber holders.

0.071 mm to 0.50 mm ± 0.038 mm in X, and from 0.67 mm ± 0.066 mm to 0.55 mm ± 0.065 mm in Y for the white and black holders, respectively. This effect is likely due to the absorption of photons in the black holder that otherwise would have reflected off of inter-fiber material in the white holder (see Fig. 1 and [13]).

C. Preliminary Imaging Results

Using the 0.5 mm thick $CaF_2(Eu)$ crystal coupled to the 1.7 mm PS light diffuser and white fiber holder with 10 cm long DCPS fibers, some preliminary images were made using ^{204}Tl (Fig. 9). Two images were collected, as the mask did not fit entirely into the FOV of the beta imaging probe, and digitally spliced together (Fig. 9B). The non-linearities, although minimal, can partially be compensated for by adjusting the gains of each MC-PMT pixel element. Image pixel resolution can be chosen depending on the image quality necessary for a given *in situ* situation.

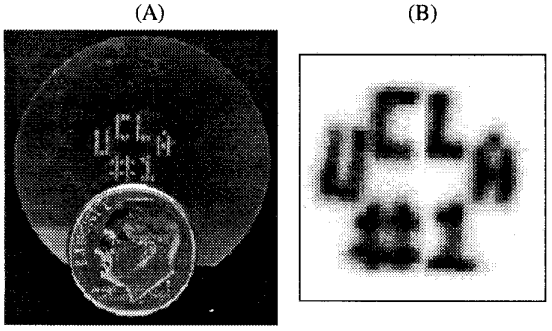

FIGURE 9. (A) Transmission phantom: 0.4 mm thick Cu plate with 0.5 mm ϕ holes spaced 0.6 mm apart horizontally and vertically. Dime is included for scale. (B) Composite image (64 x 64 pixels, 256 gray levels, 220k events) made with ^{204}Tl through transmission phantom in the 9 mm FOV.

IV. CONCLUSIONS

We are developing a small area, beta sensitive imaging device for *in situ* use. The size of the device is small enough to fit into small surgical openings while large enough to produce images of clinical value.

The best scintillator was a 0.5 mm thick x 1.25 cm ϕ $CaF_2(Eu)$ scintillator. The optimum light diffuser using a white fiber holder was found to be a 1.7 mm thick x 1.25 cm ϕ PS disk with roughened and absorbing sides. The Kuraray DCPS fibers had the best transmission properties for the $CaF_2(Eu)$ scintillator. Although the highest pulse height was achieved with a white fiber holder surrounding the bundle of 19 hexagonally arranged fibers, the best spatial resolution (0.50 mm ± 0.038 mm in X) was found with a black fiber holder which acted to absorb reflected, randomized events. Moreover, a 20% variation in pulse height, with 164% increase in PS light diffuser thickness had no significant effect on spatial resolution. For the longer (2 m) more flexible fiber bundles, larger losses, as measured for a single bundle case, are anticipated with a corresponding resolution degradation.

The discretized nature of the PD is an important aspect of the signal division. The 64 channel Philips XP1722 FO windowed MC-PMT is considered well suited as a discretized PD package for this imaging application. With the 2.54 mm pixels, this MC-PMT can measure the ~75 PEs that propagate through the imaging chain.

Previous measurements on the device sensitivity indicate that with a low threshold on the ^{204}Tl beta spectrum, the device sensitivity is ~8400 cps/μCi of radioactivity [4]. Further measurements to understand the device performance in the clinical setting are underway. Along with the achieved high spatial resolution, the beta imaging intra-operative imaging probe is sensitive to small areas and amounts of radioactivity. These performance parameters will enable a surgeon to dynamically image and identify residual radiolabeled tumor deposits for subsequent removal.

V. ACKNOWLEDGMENTS

The authors would like to thank Philips Photonics for lending the use of the XP1700 MC-PMTs, Dr. Simon Cherry, Dr. Keith Black, Esso Flyckt, and also Thomas Farquhar for helpful discussions, Drs. Jay Hauser and Yuri Bonushkin for help with the crosstalk measurements, Dr. Muzaffer Atac for providing sample fibers, Ken Meadors and Gerald Moffat for expert technical assistance, and Kuraray Int'l, Incom, Electro-Fiber Optics, Spectran, and Fiberguide for material samples. This work was funded in part by DOE contract DE-FC03-87-ER60615 and NCI grant R01-CA61037.

VI. REFERENCES

[1] TS Hikernell, HB Barber, HH Barrett, JM Woolfenden. 1988. Dual-Detector Probe for Surgical Tumor Staging. *J. Nuc. Med.* **29**(6):1101-1106.

[2] HB Barber, HH Barrett, JM Woolfenden, KJ Meyers, TS Hickernell. 1989. Comparison of *In Vivo* Scintillation Probes and Gamma Cameras for Detection of Small, Deep Tumors. *Phys. Med. Biol.* **34**(6):727-739.

[3] LR MacDonald, *et al.* 1995. Investigation of the Physical Aspects of Beta Imaging Probes Using Scintillating Fibers and Visible Light Photon Counters. *IEEE Trans. Nucl. Sci.* **NS-42**(4):1351-1357 and references therein.

[4] MP Tornai, *et al.* 1995. Development of a Small Area Beta Detecting Probe for Intra-Operative Tumor Imaging. *J. Nuc. Med.* **36**(5):109P.

[5] LR MacDonald, *et al.* 1995. Small Area, Fiber Coupled Scintillation Camera for Imaging Beta-Ray Distributions Intra-Operatively. *Proc. SPIE: Photoelectronic Detectors, Cameras and Systems.* **2551**:92-101.

[6] CS Levin, LR MacDonald, MP Tornai, EJ Hoffman, J Park. 1995. Optimizing Light Output from Thin Scintillators Used in Beta-Ray Camera for Surgical Use. Submitted to *IEEE Trans. Nucl. Sci.*

[7] MP Tornai, EJ Hoffman, LR MacDonald, CS Levin. 1995. Characterization of Fluor Concentration and Geometry in Organic Scintillators for *In Situ* Beta Imaging. Submitted to *IEEE Trans. Nucl. Sci.*

[8] B Selverstone, AK Solomon. 1948. Radioactive Isotopes in the Study of Intracranial Tumors. *Trans. Am. Neuro. Assoc.* **73**:115-119.

[9] RR Raylman, SJ Fischer, RS Brown, SP Ethier, RL Wahl. 1995. Fluorine-18-Fluorodeoxyglucose-Guided Breast Cancer Surgery with a Positron-Sensitive Probe: Validation in Preclinical Studies. *J. Nuc. Med.* **36**(10):1869-1874, and references therein.

[10] FD Rollo, Ed. 1977. *Nuclear Medicine Physics, Instrumentation, and Agents.* C.V. Mosby Company. Saint Louis. Ch. 6.

[11] HH Barrett, W Swindell, Eds. 1981. *Radiological Imaging: The Theory of Image Formation, Detection, and Processing.* Vol. 1. Academic Press. New York. Ch 5.

[12] J Bradshaw, C Burnham, J Correia, WL Rogers, NH Clinthorne. 1985. Application of Monte-Carlo Methods to the Design of SPECT Detector Systems. *IEEE Trans. Nucl. Sci.* **NS-32**(1):753-757.

[13] JS Karp, G Muehllehner. 1985. Performance of a Position-Sensitive Scintillation Detector. *Phys. Med. Biol.* **30**(7):643-655.

[14] JP O'Callaghan, R Stanek, LG Hyman. 1984. On Estimating the Photoelectron Yield and the Resultant Inefficiency of a Photomultiplier-Based Detector. *Nucl. Instr. Meth.* **225**(1):153-163.

[15] B Baumbaugh, *et al.* 1994. Performance of Multiclad Scintillating and Clear Waveguide Fibers Read Out with Visible Light Photon Counters. *Nucl. Instr. Meth.* **A345**(2):271-278.

[16] E Tanaka, T Hiramoto, N Nohara. 1970. Scintillation Cameras Based on New Position Arithmetics. *J. Nuc. Med.* **11**(9):542-547.

[17] Philips Photonics. 1993. *XP1700 Multi-Channel Photomultipliers Catalogue.*

[18] S Siegel, RW Silverman, Y Shao, SR Cherry. 1995. Simple Charge Division Readouts for Imaging Scintillator Arrays Using a Multi-Channel PMT. Submitted to *IEEE Trans. Nuc. Sci.*